8-16-2022

Designing an Interchangeable Multi-Material Nozzle System for the 3D Bioprinting Process

Cartwright Nelson
Keene State College

Slesha Tuladhar
Keene State College

MD Habib
Keene State College

Comments

This is an Accepted Manuscript of an article published by ASME in Journal of Medical Devices in 2022, Version of Record available online: https://dx.doi.org/10.1115/1.4055249

Designing an Interchangeable Multi-Material Nozzle System for the 3D Bioprinting Process

Cartwright Nelson

Department of Sustainable Product Design and Architecture, Keene State College,

229 Main Street, TDS Center, Keene, NH 03435

Carthwright.nelson@keene.edu

Slesha Tuladhar

Department of Sustainable Product Design and Architecture, Keene State College,

229 Main Street, TDS Center, Keene, NH 03435

Slesha.tuladhar@keene.edu

Ahasan Habib, Ph.D.

Department of Sustainable Product Design and Architecture, Keene State College,

229 Main Street, TDS Center, Room 121, Keene, NH 03435

md.ahasan.habib@keene.edu

ABSTRACT

Three-dimensional bioprinting is a rapidly growing field attempting to recreate functional tissues for medical and pharmaceutical purposes. Development of functional tissue requires deposition of multiple biomaterials encapsulating multiple cell types, i.e., bio-ink necessitating switching ability between bio-inks. Existing systems use more than one print head to achieve this complex interchangeable deposition, decreasing efficiency, structural integrity, and accuracy. Therefore, the objective of this paper is to develop an alternative deposition system that will not require more than one print head for multi-material bioprinting. To achieve that objective, we developed a nozzle system capable of switching between multiple bio-inks with continuous deposition, ensuring the minimum transition distance so that precise deposition transitioning can be achieved. This research progressed from a prototyping stage of nozzle system to the final selection of the system. Finally, the effect of rheological properties of different bio-material compositions on the transition distance is investigated by fabricating the sample scaffolds.

Keywords: Multi-material, 3D bio-printing, rheology, nozzle system.

1. INTRODUCTION

Bioprinting is an emerging field that has the potential to recreate 3D functional living tissue by allocating biomaterials along with high precision positioning of cells in a layer-by-layer fashion [1, 2]. Among various techniques, the extrusion-based 3D bioprinting technique can fabricate intricate and well-defined pore geometries with a single or multiple materials mimicking the native tissue architecture [3]. Due to various factors such as biocompatibility, less cytotoxicity, and high-water content (<90%), hydrogels extracted from nature are commonly considered as the bio-ink for scaffold fabrication in extrusion-based bio-printing techniques [4].

Success in tissue engineering depends on the ability to fabricate the scaffold mimicking the native tissue architecture with controlled deposition of multiple bio-materials encapsulating multiple cells [5]. Various efforts have been reported to fabricate tissue scaffolds using multi-materials and cell types [6-8]. A multi-head tissue/organ building system (MtoBS) was designed to fabricate scaffolds with polycaprolactone (PCL) and alginate with different cell types [9]. Another multi-head deposition technique was designed to fabricate a mechanically strong scaffold with synthetic polymers [10]. An Integrated Organ Printing (IOP) system consisting of multiple cartridges was used to fabricate the structure of the natural urethra of rabbits ensuring mechanical properties and better cell growth. Some other works have also been reported where multiple print heads have been used to fabricate multi-material scaffolds [11-14]. However, fabricating the scaffold with multiple materials often involves the sequential deposition of different materials. Each material deposited needs to carefully align with the subsequent nozzle and routinely create a flow of bio-ink on-demand with a lot of interruption. All of this must be done precisely, without introducing defects. Therefore, multi-head 3D bioprinters have some inherent drawbacks which increase fabrication time due to switching between multiple materials [15-17]. Moreover, switching between materials creates discontinuity which reduces the shape fidelity and eventually undermines the mechanical integrity of the final scaffold [15]. In this research, we have developed a nozzle system capable of switching between multiple hydrogels with continuous deposition through the same nozzle outlet, ensuring the minimum transition distance so that precise deposition transitioning can be achieved.

The flowability of the biomaterials, and the ability to form and hold filament geometry such as, printability, can be controlled by the rheology of the considered biomaterials [25, 26]. The viscosity of the biomaterials, which can be increased by increasing the solid content [29-31], directly impacts the printability and shape fidelity of the filament and final scaffold [27, 28]. It can also affect the transition distance for multi-material deposition [18]. It requires an extended amount of applied pressure to extrude which eventually negatively affects the cell viability [25]. Therefore, we have analyzed the effect of viscosity on the transition distance by controlling the weight percentage of the constituents of hybrid hydrogels.

2. PREPARATION OF 3D BIOPRINTER-READABLE FILE

We used a three-axis 3D bioprinter, BioX (CELLINK, Boston, MA), to fabricate the scaffold. The prepared hybrid hydrogels are stored in disposable syringes and extruded pneumatically through the same nozzle on a stationary build plane. Various printing parameters such as nozzle's internal diameter, applied air pressure, print head speed, and the perpendicular distance between the nozzle tip and print bed, commonly known as print distance can control the deposition rate of the material. The print speed, air pressure, and the perpendicular distance between the nozzle tip and print bed used in fabricating the scaffold are respectively 10 mms^{-1}, 50 kPa, and 0.405 mm unless otherwise stated. In this paper, we used the nozzle diameter of 410 µm. However, selection of nozzle diameter can be driven by material viscosity, applied pressure, print speed, and level of accuracy needed for the targeted scaffold to fabricate. All scaffolds were printed under room temperature having a plan to print cell-encapsulated material in the same

temperature condition in future. Rhino 6.0 (https://www.rhino3d.com), a computer-aided design (CAD) software, was used to design and define the vectorized toolpath of a scaffold. Slicer (https://www.slicer.org), a G-code generator software was used to generate a Bio-X compatible file including the toolpath coordinates and all process parameters to fabricate the scaffold. The material was deposited in a layer-upon-layer fashion. The physical cross-linking of the fabricated scaffold after the print was ensured by the spray of $CaCl_2$. The overall scaffold fabrication process is schematically shown in Fig. 1.

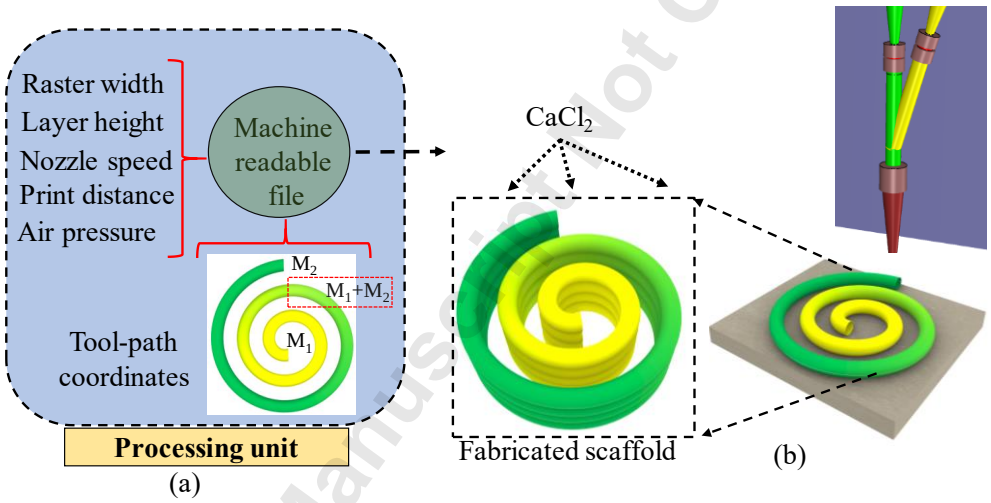

Fig. 1 (a) Preparing machine-readable file for any kind of scaffolds to print and (b) A demonstration of 3D fabrication of a spiral scaffold with multi-material through a single outlet.

3. INTERCHANGEABLE NOZZLE SYSTEM DESIGN

3.1 Initial design

The initial prototype was created by running tubing through a hollowed-out 3ml syringe and into a 410 µm nozzle. The syringe and nozzle were sealed with epoxy resin shown in Fig. 2(a). Although we were able to extrude biomaterial, it required a substantial amount of pressure to achieve the desired results. Tubing had to be small enough to fit into the nozzle. To improve the initial prototype, we designed a set of inserts instead of tubing to allow more of the syringe volume to be filled with material. Using tubing wasted a lot of space inside the syringe, so we designed inserts that allowed to utilize more space. All the prototypes were fabricated using a Stratasys Dimension 1200es 3D printer. One prototype is shown in Fig. 2(c)(i). This system took approximately 120 kPa pressure that is relatively less than the initial prototype. Since the insert was 3D printed, the desired diameter of the extrusion hole was not achieved. Moreover, its inner surface was rough due to the staircase effect. This may hinder the smooth flow of the hydrogel material and eventually increase the required pressure. Another insert was designed and fabricated as shown in Fig. 2c(ii) to separate the material into the dispensing syringe reducing the total contact surface between nozzle wall and material. This prototype was tested using the Cellink BioX 3D bioprinter by extruding various hydrogel materials such as CELLINK starter ink and a composition with 6% alginate and 6% Carboxymethyl Cellulose (CMC). Scaffold having a different internal geometry was fabricated shown in Fig. s 3a(iii) and 3b(i). This prototype showed promising results with some adjustments. All fabricated scaffolds were submerged into $CaCl_2$ for 2-3 minutes to crosslink. Even authors were able to print various scaffolds with multiple materials using this insert, scaffolds suffered to retain shape fidelity in post-printing stage. For an example, it showed a filament width change of

350±36%, pore diffusion rate 135±23%, and printability 0.7-1.19. Since, this insert needed uncontrolled higher applied pressure to extrude materials, it created non-uniform material deposition as shown in Fig. 3a(iii). It was noticed that crosslinking those scaffolds in post-printing stage helped retain a filament width change ranging from 195±15%. Pore diffusion rate 78±11%, and printability 0.78-1.07. There was also an issue of backflow where instead of extruding material, the pressure from one side of the system pushed the material into the other side of the system. To correct this issue, another setup was prepared including check valves. After adding check valves, the pressure would build up in the system which caused the material to continue to deposit after the pressure had been shut off. The system was also very difficult to clean. All these challenges led to the development of the current system being tested.

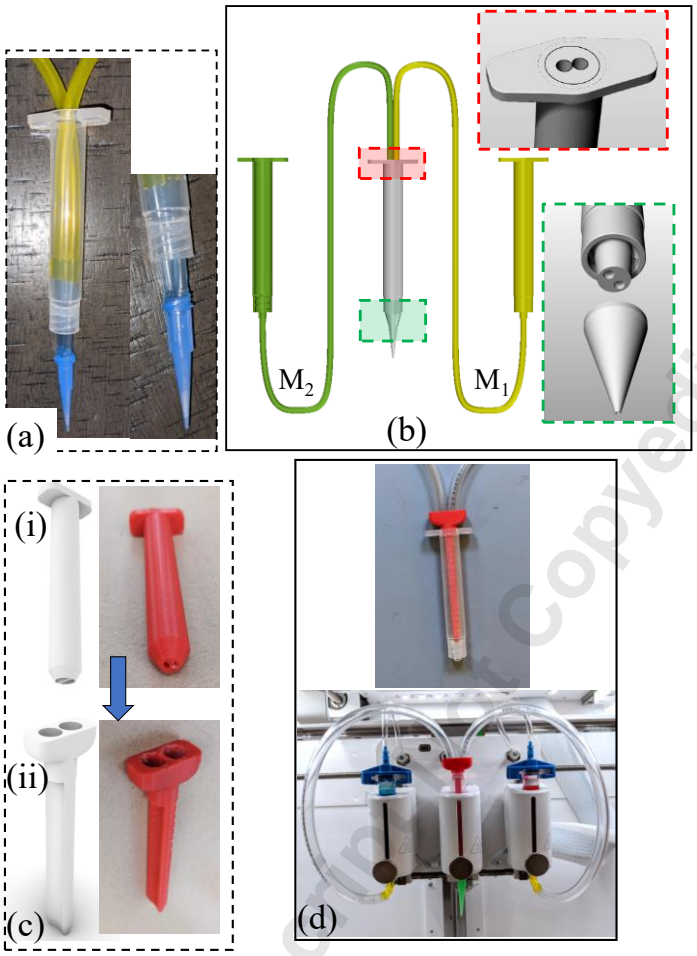

Fig. 2 Progression of the nozzle system design process: (a) Inserting two tubes into dispensing nozzle, (b) Computer aided design of a prototype nozzle system, (c) 3D printed inserts having two material flow system, and (d) Final setup with 3D printed attachment to fabricate scaffold.

3.2 Final design

Prototypes of the nozzle system designed and fabricated as shown in Fig. 3 motivated us to design a robust nozzle system that will be easier to build, clean, control, and require less pressure to extrude. To build such a nozzle system, we used a medical-grade Y-connector (4 cm length, 30^0 angle between two syringe connectors with standard

threads) with two female Leur-lock inputs (2.44 cm length, 1.12 cm external diameter) and a single male Leur-lock output (Qosina, Ronkonkoma, NY). Duckbill check valves (Qosina, Ronkonkoma, NY) were attached to the female ends of the Y-connector with the other ends connected to 3ml dispensing syringes (EFD, Nordson, East Province, RI). The entire nozzle system is shown in Fig. 5(a). Dispensing nozzles were connected separately with two different printheads of the BioX 3D printer. Having a free-spinning male Leur-lock on the output of the Y-connector allows the system to be used interchangeably with any nozzle size and type. The final nozzle setup with the printer is shown in Fig. 5(b). Various scaffolds with different geometries and infill densities (50-60%) having eight layers were fabricated using this designed nozzle system as shown in Fig. s 3a(ii), 3b(iii), and 3c(ii). Each bilayer was fabricated with yellow and green colored material (the composition of 6% alginate and 6% CMC was separated by yellow and green food color). The scaffold demonstrates good shape fidelity. For an example, printing the same scaffolds as shown in Fig. 3a(ii) with the final setup took lower amount of pressure which showed comparatively uniform material deposition and a filament width improvement of 50% compared to the scaffold fabricated using our previously designed insert.

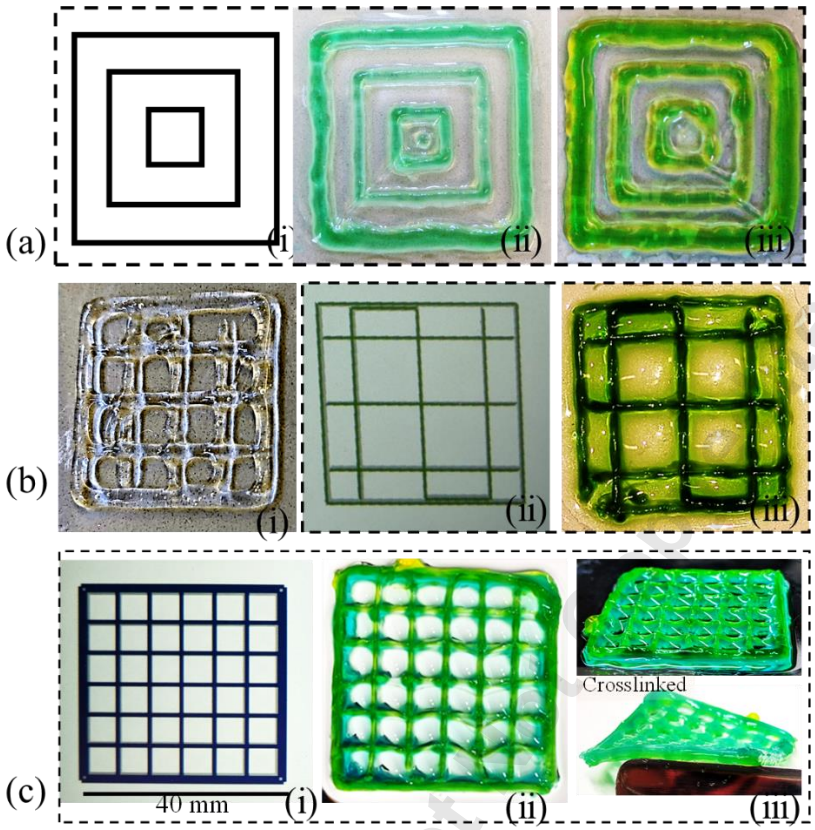

Fig. 3 **Scaffold (a) fabricated with insert shown in Fig. 2(c)(ii) with composition 6% alginate-6% CMC, (b-c) fabricated with our proposed nozzle system with two different materials and crosslinked after fabrication.**

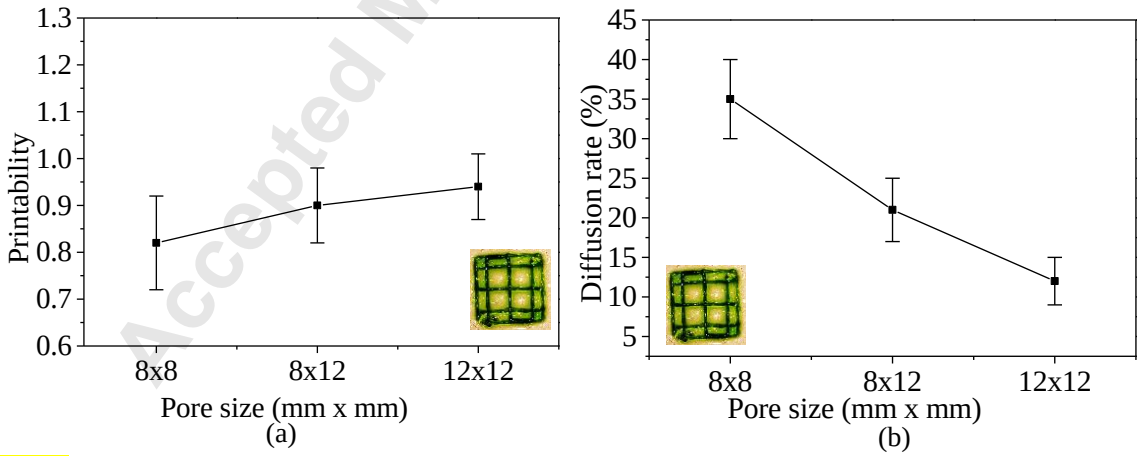

Fig. 4 **(a) Printability and (b) shape fidelity of various pore sizes of the scaffold shown in Fig. 3b(iii) fabricated with composition 6% alginate 6% CMC.**

Shape fidelity of the fabricated filament was assessed with respect to the designed filament width. Fig. 4 shows the printability and diffusion rate [19] of various pore sizes of the scaffold shown in Fig. 3b(iii). It is clear from this figure that with increasing the size of the pore, the printability and shape fidelity were improved from 0.81 to 0.94 and 34% to 12%, respectively. Since the nozzle size used in this paper was 410 µm, we observed an overall 35% deviation of the filament width with respect to 410 µm of the scaffold shown in Fig. 3c(ii). It also did not showed filament sagging which consequently helped achieving a defined top surface and build height as shown in Fig. 3c(iii). However, this deviation may vary depending on the material viscosity, nozzle diameter, applied pressure, and print distance [19]. For an example, we proposed a high-viscous clay-based biomaterial compositions prepared with 4% alginate, 4% CMC, 3% Montmorillonite (MMT) nano-clay that showed 3-5% diffusion rate for various pore sizes ranging from 2-5 mm with 10 psi applied pressure and 0.7 mm printing distance extruded through 410 µm nozzle [20]. In future, authors plan to use this composition and optimize related printing process parameters such as material compositions, nozzle size, applied pressure, to achieve defined filament width and pore sizes and geometries using our proposed nozzle system. Engineered tissues must be supplied with sufficient amount of oxygen, nutrients, and remove waste materials. Oxygen supply can be achieved through macro-porosity such as pore size and geometries and internal micro-porosity [21, 22]. Various biomaterials have various level of internal micro-porosity [23, 24]. In order to achieve sufficient amount of oxygen diffusion, a systematic pore size and geometry distributions along with materials with suitable internal porosity can help [23, 24]. In our earlier works, we reported various

toolpath designs to achieve various pore size and geometries and biomaterial compositions with various internal porosities [19, 25].

A scaffold of spiral shape was fabricated with two different materials (the composition of 6% alginate and 6% CMC was separated by yellow and green food color) shown in Fig. 5(b). It required approximately 50 kPa which is significantly less pressure than the previous prototypes. A comparison of required pressure between the proposed nozzle system shown in Fig. 5(a) and the prototypes shown in Fig. 2 is tabulated in Table 1.

Table 1 Percentage of reduction of required pressure of the proposed nozzle system with respect to the prototypes shown in Fig. 2.

	Prototypes		
	1	2	3
Required Pressure (kPa) for prototype	120	100	80
Required Pressure (kPa) for proposed	50	50	50
% Reduction of required pressure	140	100	60

4. VALIDATION OF THE NOZZLE SYSTEM

4.1 Hydrogel preparation

The biomaterials used for our nozzle system verification and scaffold fabrications were alginate (alginic acid sodium salt from brown algae; Sigma-Aldrich, St. Louis, MO, USA) and low viscous carboxymethyl cellulose (CMC) (pH: 6.80) (Sigma-Aldrich). Alginate is a highly used biopolymer, composed of (1-4)-linked β-Dmannuronic (M) and α-

Lguluronic acids (G). This material is soluble in water, because it is negatively charged linear copolymer (M and G blocks). It also supports cell growth and exhibits high biocompatibility. Combining other materials with alginate can help recreate tissue [1, 26]. Carboxymethylcellulose (CMC), a derivative of cellulose, is also water-soluble biopolymer. This copolymer is formed by two monomers such as, β-D-glucose and β-D-glucopyranose-2-O-(carboxymethyl)-monosodium salt which is connected via β-1,4-glucosidic bonds [27]. This material is widely used as a thickener and it is non-toxic and non-allergenic [28]. It has been reported that the binding of CMC's matrix protein assists in cell migration and cell attachment [29]. Moreover, alginate-CMC (Alg-CMC) hybrid hydrogel has been used to fabricate beads for various drug delivery experiments [30]. Various weight percentages of alginate and CMC were used to prepare five different hybrid hydrogel samples maintaining the total solid content 8% (w/v) shown in Table 2. Food colors were used to differentiate the compositions. To mix the solution uniformly, a magnetic stirrer was used.

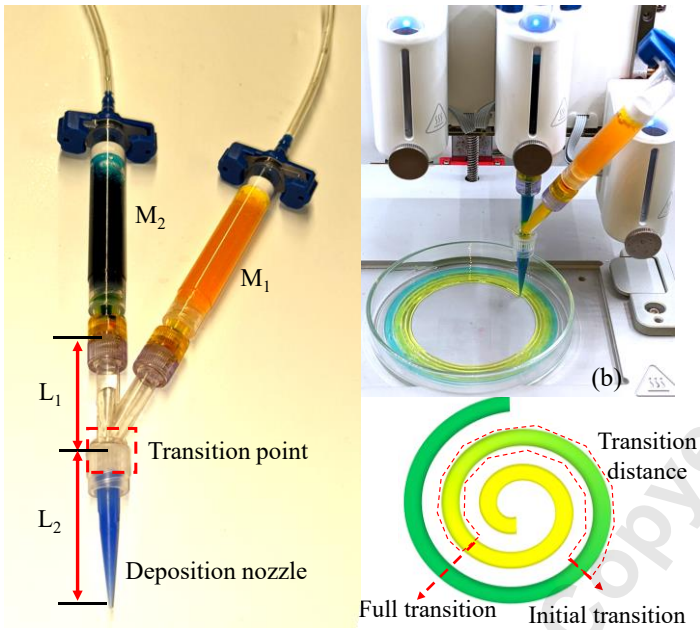

Fig. 5 (a) Modified nozzle system, and (b) Deposition with modified nozzle system, and (c) Schematical representation of transition distance.

Table 2 Composition with weight percentages.

Sample	Alginate (A)	CMC (C)	A/C (%)
A_8C_0	8	0	100/0
A_6C_2	6	2	75/25
A_4C_4	4	4	50/50
A_2C_6	2	6	25/75
A_0C_8	0	8	0/100

4.2 Rheological experiment

To validate our designed nozzle system, we used a set of biomaterial compositions shown in Table 2 with different rheological properties. To determine the rheological properties of all the hydrogel compositions, we used a rotational rheometer (MCR 102, Anton Paar, Graz, Austria) with parallel plate geometry (25.0 mm flat plate). We recorded

the measurements at room temperature (25^0C) with a 1.0 mm plate-plate gap. We conducted the rheological measurement at room temperature because our extrusion process is performed at room temperature, which also facilitates the quick gelation of the deposited filament [31]. The viscosities and shear stress of different concentrations were measured using a steady rate sweep test with a range of strain rate of 0.1 to 100 s^{-1}. The result of rheological properties is shown in Fig. 6.

The shear-thinning properties, i.e., the phenomenon of reducing the viscosity with increasing the shear strain on hydrogels, is crucial for extruding material through a smaller diameter nozzle [32]. Hydrogels with higher viscosity experience higher shear stress during extrusion through a nozzle, which adversely affects the encapsulated cell. Viscosity is measured for all the hybrid hydrogels shown in Table 2 with respect to various shear strain rates. Viscosity decreases with increasing the shear strain rate, that indicates all five compositions have shear thinning properties shown in Fig. 6. Pure 8% alginate showed the lowest viscosity. The viscosity increases when the percentage of CMC into the composition is increased. However, at shear strain rate of 1.0 s^{-1}, A_2C_6 showed the highest viscosity. This composition may create the highest number of hydrogen and polar bonds due to more easily accessible bond sites of polar carbonyl groups ($C^{\delta+} = O^{\delta-}$) which drives toward a high rate of cross-linking.

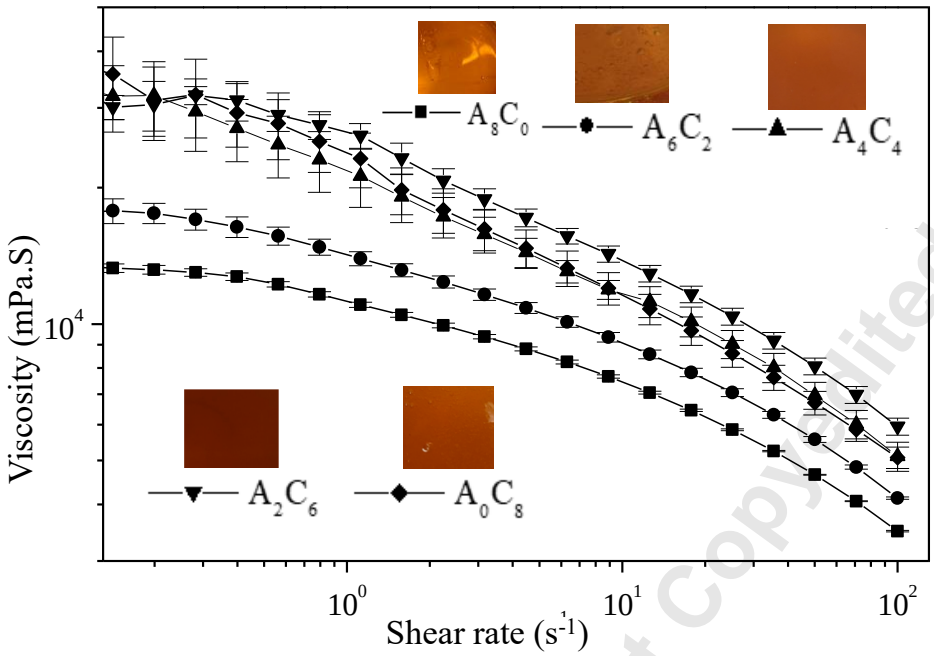

Fig. 6 Viscosities of various compositions with respect to shear rate. Pure 8% alginate showed the lowest viscosity. Normally, percentage of CMC increases viscosity into the composition. At shear strain rate of 1.0 s^{-1}, A_2C_6 showed the highest viscosity.

4.3 Measuring transition distance

To determine the transition distance, we started to extrude material 2 (blue color, M2) when the extrusion nozzle was full of material 1 (yellow color, M1). The initial transition is what the color of the second material first appears from the nozzle. Here, we defined the event as "initial transition" when the color started to turn into blue from yellow. Finally, when the extruded material turned fully to blue and no longer yellow color was extruded from the nozzle, the event was defined as "Full transition". The distance between the initial transition and full transition was defined as "transition distance". The transition points were determined by human measurement and timing with a stopwatch.

It is true that this method is susceptible to human error, and knowing this, the transition test was conducted at least three times for each composition and the results were then averaged. This helps eliminate some of the human error. In future, this would be done with image processing software that can detect and analyze RGB values and precisely determine the transition position. All events and transition distance are schematically shown in Fig. 5 (c) in section 4.1.

A spiral toolpath is designed having a starting and ending diameter of 80mm and 2mm respectively, with 20 turns using Rhino 6 CAD software as shown in Fig. 7, although printing was stopped after full transition, so the entire spiral was not printed. The proposed nozzle system was used to extrude all five types of hybrid hydrogels to fabricate that spiral scaffold. Before printing, material from one of the syringes was extruded until it filled the whole nozzle system. The other syringe was then used to print the spiral and the amount of time it took for the color to initially appear as well as to fully transition were recorded in seconds, which is shown in Fig. 7. Times were multiplied by the print speed to calculate the distance between the initial color change and the full color change. The difference between the initial and full color changes was used to determine the transition difference. To save time, two different printing programs were set up, one using the first tool for extrusion and the other using the third tool. This allowed us to easily switch between the two each time instead of having to extrude the second material before each print. A minimum of five trials (n=5) was conducted with each concentration of biomaterial maintaining all other parameters as constant. This calculated information from each of the trials was used to find the average initial transition distance, average full

transition distance, and average difference distance for each concentration tested. We presented all the data in a form of mean ± standard deviation. To assess the statistical significance of differences in transition distance, we considered the distribution of values is normal. A two-way ANOVA and a significance level of p = 0.05 were used to determine the statistically significant differences. Minitab18.0 and OriginPro 5.0 two statistical software were used to do the quantitative and graphical analysis.

We used a single and multiple filament system to determine the transition distance as shown in Fig. 8. In multiple filament system, we used a filament-to-filament distance of 2 mm. Fig. 9(a) represents the initial, full, and actual transition distances separately. Fig. 9(b) shows them stacked so that the total transition information can be seen. The second in this figure is quite important for this experiment, because the best concentration will ultimately be the one with the shortest transition distance for all three categories. Based on the data collected, A_2C_6 has the shortest transition distance for all three categories, making it the best overall concentration for this system. With A_2C_6, the initial transition and full transition distances increase as the percent of CMC increases and percent alginate decreases. This is most likely due to the thickening properties or the viscosity increase. Surprisingly, the trend is not consistent with A_8C_0, indicating CMC must have some benefit in small concentrations or, alginate on its own is more sticky than viscous. The initial transition is also mostly viscosity dependent except A_8C_0. Therefore, a small portion of CMC is likely to increase the followability and eventually assist material transition better where a larger proportion of CMC, i.e., high-viscous hydrogel, can create difficulty with a smooth transition in a single nozzle deposition system.

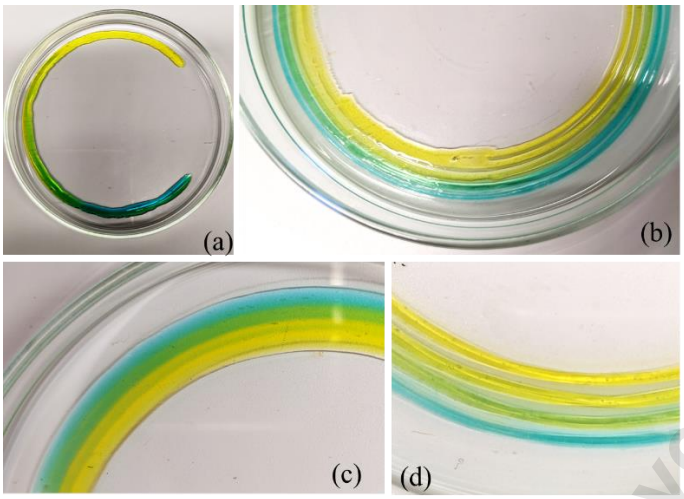

Fig. 7 **Determining transition distance using various scenario: (a) Single filament, multiple filament system with a filament-to-filament distance of 2 mm printed with material (b) A_2C_6, (c) A_8C_0, and (d) A_0C_8.**

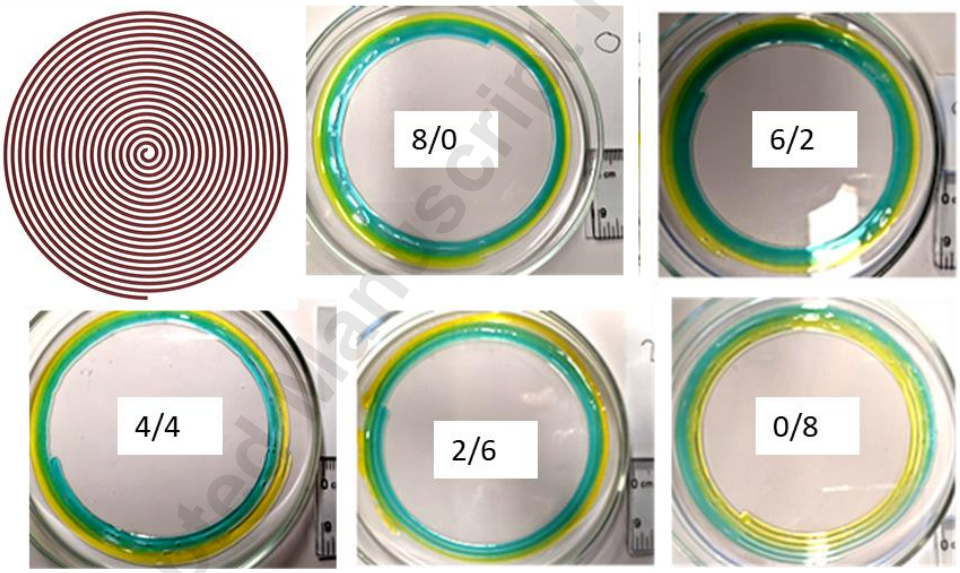

Fig. 8 **Determining transition distance of various compositions having various viscosities. With increasing the percentage of CMC, we observed defined filament geometries.**

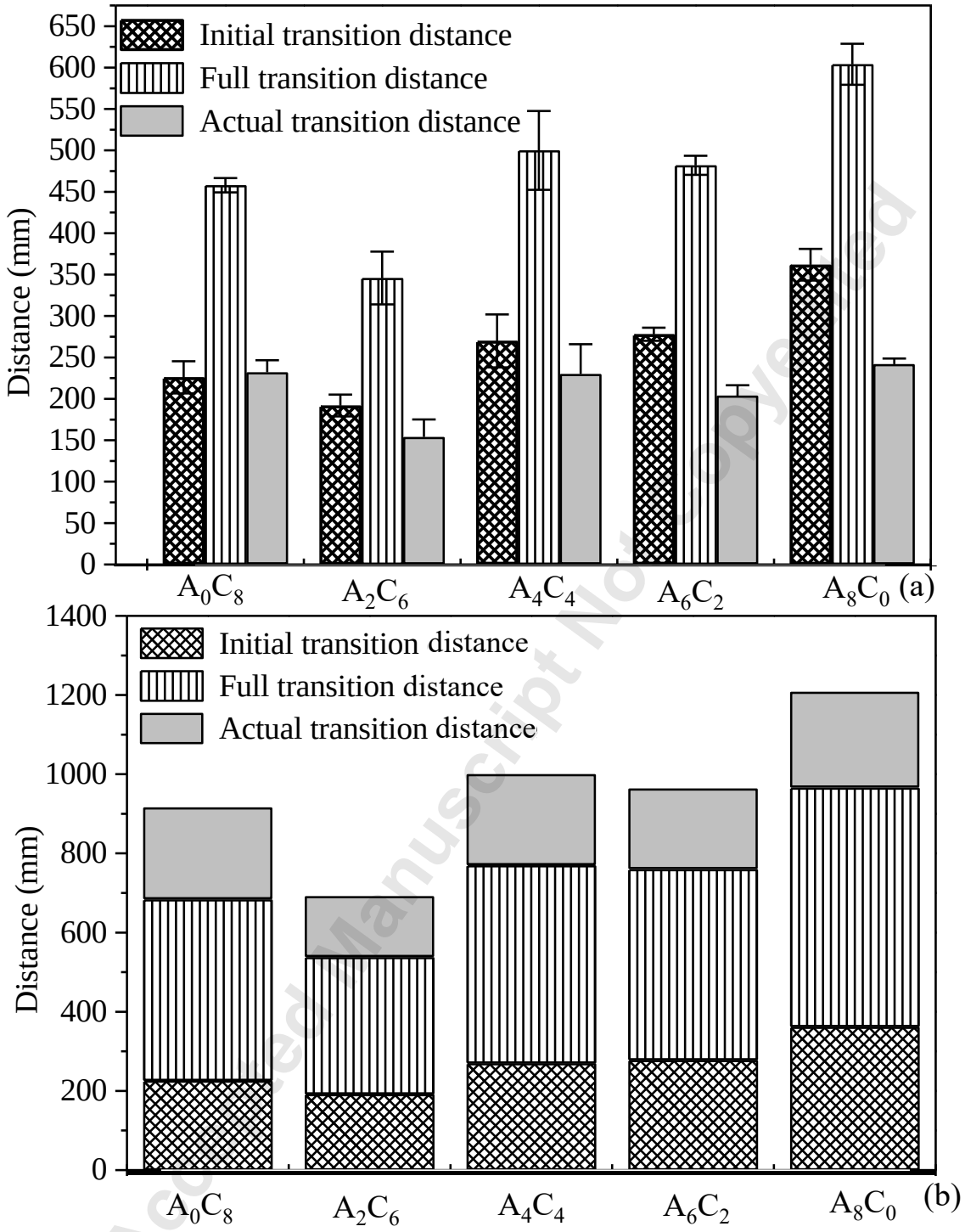

Fig. 9 (a) Results of transition distance with respect to the initial and full transition for various compositions. (b) a comparative representation of initial, full, and actual transition distance.

5. DISCUSSION

Hydrogels prepared with various polymers extracted from nature, such as alginate, collagen, gelatin, chitosan, cellulose, etc., were successfully used for bioprinting [33-35]. However, achieving the stability and maintaining the shape fidelity of the 3D printed scaffold with a great spatial control is still challenging [31, 36]. Attempting to print with multiple biomaterials ensuring material transition, scaffold geometry, and good cell viability adds more roadblocks toward a successful tissue fabrication [2]. An interchangeable nozzle system with easy material transition and less required pressure can offer a good solution. Therefore, a nozzle system which is easier to build, clean, and control the material transition was designed, prototyped, built, and validated in this paper. It also requires less pressure to extrude which will protect encapsulated cells during extrusion and eventually good cell viability. Moreover, this system can extrude materials with various viscosities. The addition of co-axial nozzles with this interchangeable system can help the scaffold fabrication with vascularity and a successful tissue fabrication in long run. A conical structure including three materials supply system with a common intersection to extrude the material can help add more variation with the proposed system. The effect of the material viscosity on various transition scenarios was analyzed with our proposed nozzle system. If the initial or full distance is too large, it will be more challenging to time the transition in a real scaffold bio-print. Even when the initial transition is very small, if the transition difference is too large, the deposition will not be precise enough for functional tissue or any type of bio-print. A large transition difference could be useful when printing functional gradients, but that is not the goal of this

research. An interconnected system ensuring crosstalk between the hardware and software systems to manage the user-defined fabrication recipe is ongoing in our research. The intent of the paper was to demonstrate a multi-material nozzle system capable of transitioning between materials without discontinued material deposition. The materials being used at the time were not what was being proposed. In current works, the authors have demonstrated that their new materials can achieve a high printability with excellent shape fidelity and structural integrity [37]. The nozzle system can print any materials that the traditional system is able to print. It shows its ability to transition and can therefore be a suitable option for large-scale scaffold fabrication with better materials. The future direction of this research is to use a surface modifier such as a superhydrophobic coating in the Y-connector to assist in smooth material transition. Moreover, controlling the overall length L (L1+L2), using a dispensing nozzle with a shorter length, can reduce the transition distance, which will also be analyzed in the future. Finally, various hydrogels encapsulating multiple cells will be extruded and analyzed to validate this proposed nozzle system.

6. CONCLUSION AND FUTURE WORK

We have demonstrated the development of an interchangeable nozzle system for a 3D bioprinting technique to fabricate scaffolds with multiple hydrogels. The proposed nozzle system can interchange the deposition of multiple hydrogels smoothly through a single nozzle. This system allows the deposition and transition of hydrogels having various viscosities. As we know, most of the tissues require multiple cell types to regenerate, this system can be helpful allowing the extrusion of multiple materials encapsulating multiple

cell types. Moreover, extruding through a single outlet with interchangeable feature can assist achieving dimensional accuracy, less time to print, and seamless transition. It is believed that further improvements of this proposed interchangeable nozzle system will contribute to enhancing the ability to fabricate scaffolds having complex internal and external geometry. As a part of this effort, we will continue our research to find right kind of material compositions and process parameters suitable for this system. Recently, we published a hybrid pre-crosslinking approach to get better shape fidelity of full-scale scaffolds ensuring internal and external geometries, and conducted a bacterial growth test on pre-crosslinked hydrogels [37]. In future, we will use the same material compositions to extrude through this interchangeable nozzle system to identify any variations in terms of bacterial growth. Moreover, we plan to encapsulate hMSC, epithelial, and endothelial cells in our already proposed materials [19, 25, 37] and extrude through this interchangeable nozzle system to record the cell actions.

ACKNOWLEDGEMENTS

Research was supported by New Hampshire-EPSCoR through BioMade Award #1757371 from National Science Foundation and New Hampshire-INBRE through an Institutional Development Award (IDeA), P20GM103506, from the National Institute of General Medical Sciences of the NIH.

REFERENCES

[1] S. Ahn, H. Lee, and G. Kim, 2013, "Functional cell-laden alginate scaffolds consisting of core/shell struts for tissue regeneration," *Carbohydrate polymers*, vol. 98, no. 1, pp. 936-942.

[2] Z. Wang, S. J. Lee, H.-J. Cheng, J. J. Yoo, and A. Atala, 2018, "3D bioprinted functional and contractile cardiac tissue constructs," *Acta biomaterialia*, vol. 70, pp. 48-56.

[3] H.-J. Kong, K. Y. Lee, and D. J. Mooney, 2002, "Decoupling the dependence of rheological/mechanical properties of hydrogels from solids concentration," *Polymer*, vol. 43, no. 23, pp. 6239-6246.

[4] K. Markstedt, A. Mantas, I. Tournier, H. c. Martínez Ávila, D. Hägg, and P. Gatenholm, 2015, "3D bioprinting human chondrocytes with nanocellulose–alginate bioink for cartilage tissue engineering applications," *Biomacromolecules*, vol. 16, no. 5, pp. 1489-1496.

[5] D. B. Kolesky, K. A. Homan, M. A. Skylar-Scott, and J. A. Lewis, 2016, "Three-dimensional bioprinting of thick vascularized tissues," *Proceedings of the National Academy of Sciences*, vol. 113, no. 12, pp. 3179-3184.

[6] Bertassoni LE, Cecconi M, Manoharan V, Nikkhah M, Hjortnaes J, Cristino AL, Barabaschi G, Demarchi D, Dokmeci MR, Yang Y, Khademhosseini A., 2014, "Hydrogel bioprinted microchannel networks for vascularization of tissue engineering constructs". Lab on a Chip. 14(13):2202-11.

[7] Zhang YS, Arneri A, Bersini S, Shin SR, Zhu K, Goli-Malekabadi Z, Aleman J, Colosi C, Busignani F, Dell'Erba V, Bishop C., 2016, "Bioprinting 3D microfibrous scaffolds for engineering endothelialized myocardium and heart-on-a-chip", Biomaterials, 110:45-59.

[8] Nadernezhad, Ali, Navid Khani, Gözde Akdeniz Skvortsov, Burak Toprakhisar, Ezgi Bakirci, Yusuf Menceloglu, Serkan Unal, and Bahattin Koc, 2016, "Multifunctional 3D printing of heterogeneous hydrogel structures." Scientific reports 6, no. 1: 1-12.

[9] J.-H. Shim, J.-S. Lee, J. Y. Kim, and D.-W. Cho, 2012, "Bioprinting of a mechanically enhanced three-dimensional dual cell-laden construct for osteochondral tissue engineering using a multi-head tissue/organ building system," *Journal of Micromechanics and Microengineering*, vol. 22, no. 8, p. 085014.

[10] Xu, Tao, Kyle W. Binder, Mohammad Z. Albanna, Dennis Dice, Weixin Zhao, James J. Yoo, and Anthony Atala, 2012, "Hybrid printing of mechanically and biologically improved constructs for cartilage tissue engineering applications." Biofabrication 5, no. 1: 015001.

[11] J. Kundu, J. H. Shim, J. Jang, S. W. Kim, and D. W. Cho, 2015, "An additive manufacturing-based PCL–alginate–chondrocyte bioprinted scaffold for cartilage tissue engineering," *Journal of tissue engineering and regenerative medicine*, vol. 9, no. 11, pp. 1286-1297.

[12] Miri AK, Nieto D, Iglesias L, Goodarzi Hosseinabadi H, Maharjan S, Ruiz-Esparza GU, Khoshakhlagh P, Manbachi A, Dokmeci MR, Chen S, Shin SR., 2018, "Microfluidics-enabled multimaterial maskless stereolithographic bioprinting", Advanced Materials. 30(27):1800242.

[13] S. Sakai, K. Ueda, E. Gantumur, M. Taya, and M. Nakamura, 2018, "Drop-On-Drop Multimaterial 3D Bioprinting Realized by Peroxidase-Mediated Cross-Linking," *Macromolecular rapid communications*, vol. 39, no. 3, p. 1700534.

[14] L. Ruiz-Cantu, A. Gleadall, C. Faris, J. Segal, K. Shakesheff, and J. Yang, 2020, "Multi-material 3D bioprinting of porous constructs for cartilage regeneration," *Materials Science and Engineering: C*, vol. 109, p. 110578.

[15] E. Sodupe-Ortega, A. Sanz-Garcia, and C. Escobedo-Lucea, 2018, "Accurate calibration in multi-material 3D bioprinting for tissue engineering," *Materials*, vol. 11, no. 8, p. 1402.

[16] D. B. Kolesky, R. L. Truby, A. Gladman, T. A. Busbee, K. A. Homan, and J. A. Lewis, 2014, "3D bioprinting of vascularized, heterogeneous cell-laden tissue constructs," *Advanced materials*, vol. 26, no. 19, pp. 3124-3130.

[17] Maiullari F, Costantini M, Milan M, Pace V, Chirivì M, Maiullari S, Rainer A, Baci D, Marei HE, Seliktar D, Gargioli C, 2018, A multi-cellular 3D bioprinting approach for vascularized heart tissue engineering based on HUVECs and iPSC-derived cardiomyocytes. Scientific reports. 10;8(1):1-5.

[18] J. O. Hardin, T. J. Ober, A. D. Valentine, and J. A. Lewis, 2015, "Microfluidic printheads for multimaterial 3D printing of viscoelastic inks," *Advanced materials*, vol. 27, no. 21, pp. 3279-3284.

[19] A. Habib, V. Sathish, S. Mallik, and B. Khoda, 2018, "3D printability of alginate-carboxymethyl cellulose hydrogel," *Materials*, vol. 11, no. 3, p. 454.

[20] A. Habib and B. Khoda, "Development of clay based novel hybrid bio-ink for 3D bio-printing process, 2019, " *Journal of Manufacturing Processes*, vol. 38, pp. 76-87.

[21] "Bioprinting Pattern-Dependent Electrical/Mechanical Behavior of Cardiac Alginate Implants: Characterization and Ex Vivo Phase-Contrast Microtomography Assessment," *Tissue Engineering Part C: Methods*, vol. 23, no. 9, pp. 548-564, 2017, doi: 10.1089/ten.tec.2017.0222.

[22] S. Sultan and A. P. Mathew, 2018, "3D printed scaffolds with gradient porosity based on a cellulose nanocrystal hydrogel," *Nanoscale*, vol. 10, no. 9, pp. 4421-4431.

[23] L. Moroni, J. De Wijn, and C. Van Blitterswijk, 2005, "Three-dimensional fiber-deposited PEOT/PBT copolymer scaffolds for tissue engineering: Influence of porosity, molecular network mesh size, and swelling in aqueous media on dynamic mechanical properties," *Journal of biomedical materials research Part A*, vol. 75, no. 4, pp. 957-965.

[24] M. Miron-Mendoza, J. Seemann, and F. Grinnell, 2010, "The differential regulation of cell motile activity through matrix stiffness and porosity in three dimensional collagen matrices," *Biomaterials*, vol. 31, no. 25, pp. 6425-6435.

[25] M. Habib and B. Khoda, 2020, "Fiber Filled Hybrid Hydrogel for Bio-Manufacturing," *Journal of Manufacturing Science and Engineering*, pp. 1-38.

[26] E. Axpe and M. L. Oyen, 2016, "Applications of alginate-based bioinks in 3D bioprinting," *International journal of molecular sciences*, vol. 17, no. 12, p. 1976.

[27] Y. Han and L. Wang, "Sodium alginate/carboxymethyl cellulose films containing pyrogallic acid: physical and antibacterial properties," *Journal of the Science of Food and Agriculture*, vol. 97, no. 4, pp. 1295-1301, 2017.

[28] W. Tongdeesoontorn, L. J. Mauer, S. Wongruong, P. Sriburi, and P. Rachtanapun, 2011, "Effect of carboxymethyl cellulose concentration on physical properties of biodegradable cassava starch-based films," *Chemistry Central Journal*, vol. 5, no. 1, p. 6.

[29] Garrett Q, Simmons PA, Xu S, Vehige J, Zhao Z, Ehrmann K, Willcox M., 2007, Carboxymethylcellulose binds to human corneal epithelial cells and is a modulator of corneal epithelial wound healing. Investigative ophthalmology & visual science, 1;48(4):1559-67.

[30] T. Agarwal, S. G. H. Narayana, K. Pal, K. Pramanik, S. Giri, and I. Banerjee, 2015, "Calcium alginate-carboxymethyl cellulose beads for colon-targeted drug delivery," *International journal of biological macromolecules*, vol. 75, pp. 409-417.

[31] L. Ouyang, R. Yao, Y. Zhao, and W. Sun, 2016, "Effect of bioink properties on printability and cell viability for 3D bioplotting of embryonic stem cells," *Biofabrication*, vol. 8, no. 3, p. 035020.

[32] H. Li, Y. J. Tan, K. F. Leong, and L. Li, 2017, "3D bioprinting of highly thixotropic alginate/methylcellulose hydrogel with strong interface bonding," *ACS applied materials & interfaces*, vol. 9, no. 23, pp. 20086-20097.

[33] R. E. Abouzeid, R. Khiari, D. Beneventi, and A. Dufresne, 2018, "Biomimetic mineralization of three-dimensional printed alginate/TEMPO-oxidized cellulose nanofibril scaffolds for bone tissue engineering," *Biomacromolecules*, vol. 19, no. 11, pp. 4442-4452.

[34] Di Giuseppe M, Law N, Webb B, Macrae RA, Liew LJ, Sercombe TB, Dilley RJ, Doyle BJ, 2018, "Mechanical behaviour of alginate-gelatin hydrogels for 3D bioprinting", Journal of the mechanical behavior of biomedical materials. 1;79:150-7.

[35] Diamantides N, Wang L, Pruiksma T, Siemiatkoski J, Dugopolski C, Shortkroff S, Kennedy S, Bonassar LJ., 2017, "Correlating rheological properties and printability of collagen bioinks: the effects of riboflavin photocrosslinking and pH". Biofabrication, 9(3):034102.

[36] Chung JH, Naficy S, Yue Z, Kapsa R, Quigley A, Moulton SE, Wallace GG, 2013, "Bio-ink properties and printability for extrusion printing living cells", Biomaterials Science, 1(7):763-73.

[37] C. Nelson, S. Tuladhar, L. Launen, and M. Habib, 2021, "3D Bio-Printability of Hybrid Pre-Crosslinked Hydrogels," *International Journal of Molecular Sciences*, vol. 22, no. 24, p. 13481.

List of the Figures

Fig. 1 (a) Preparing machine-readable file for any kind of scaffolds to print and (b) A demonstration of 3D fabrication of a spiral scaffold with multi-material through a single outlet.

Fig. 2 Progression of the nozzle system design process: (a) Inserting two tubes into dispensing nozzle, (b) Computer aided design of a prototype nozzle system, (c) 3D printed inserts having two material flow system, and (d) Final setup with 3D printed attachment to fabricate scaffold.

Fig. 3 Scaffold (a) fabricated with insert shown in Fig. 2(c)(ii) with composition 6% alginate-6% CMC, (b-c) fabricated with our proposed nozzle system with two different materials and crosslinked after fabrication.

Fig. 4 (a) Printability and (b) shape fidelity of various pore sizes of the scaffold shown in Fig. 3b(ii) fabricated with composition 6% alginate 6% CMC.

Fig. 5 (a) Modified nozzle system, and (b) Deposition with modified nozzle system, and (c) Schematical representation of transition distance.

Fig. 6 Viscosities of various compositions with respect to shear rate. Pure 8% alginate showed the lowest viscosity. Normally, percentage of CMC increases viscosity into the composition. At shear strain rate of 1.0 s^{-1}, A_2C_6 showed the highest viscosity.

Fig. 7 Determining transition distance using various scenario: (a) Single filament, multiple filament system with a filament-to-filament distance of 2 mm printed with material (b) A_2C_6, (c) A_8C_0, and (d) A_0C_8

Fig. 8 Determining transition distance of various compositions having various viscosities. With increasing the percentage of CMC, we observed defined filament geometries.

Fig. 9 (a) Results of transition distance with respect to the initial and full transition for various compositions. (b) a comparative representation of initial, full, and actual transition distance.

List of the Tables